RP Materials: Proceedings (e-ISSN: 2583-8342)
Vol. 5, Part 1 (2026) pp. 30–35

RESEARCH PLATEAU PUBLISHERS

Cite this article: A.S. Soubhagya, K. Joy, Bio-glass nanoparticles loaded carboxymethyl pullulan 3D scaffold for bone tissue engineering, *RP Materials: Proceedings* Vol. 5, Part 1 (2026) pp. 30–35.

Original Research Article

Bio-glass nanoparticles loaded carboxymethyl pullulan 3D scaffold for bone tissue engineering

A.S. Soubhagya[1,*], Kiran Joy[2]

[1]Department of Chemistry, Govt. Model Engineering College, Thrikkakara, Ernakulam 682 021, Kerala, India
[2]Department of Chemistry, Hindustan Institute of Technology and Science, Padur, Chennai 600 103, Tamilnadu, India
[*]Corresponding author, E-mail: soubhagya.as@gmail.com

[**]Selection and Peer-Review under responsibility of the Scientific Committee of the 4th International Conference on Recent Trends in Materials Science & Devices 2026 (ICRTMD 2026) held at JVMGRR College, Charkhi Dadri, Haryana, India during 6–8 April 2026.

ARTICLE HISTORY
Received: 17 April 2026
Revised: 27 May 2026
Accepted: 27 May 2026
Published online: 12 June 2026

KEYWORDS
Carboxymethyl pullulan;
Bio-glass nanoparticles;
Bone Tissue Engineering.

ABSTRACT
Bone tissue engineering (BTE), which offers creative solutions for the repair and regeneration of complicated bone lesions, has emerged as a potential strategy to get around the drawbacks of conventional bone grafting techniques. In this study, we used freeze-drying techniques to formulate a three-dimensional (3D) porous scaffold composed of carboxymethyl pullulan (Cmp) and optimised concentration of bio-glass nanoparticles (Bg). This composite scaffold was intended to improve mechanical strength and by analysing in vitro degradation and compression strength. Several analytical methods, including FTIR, XRD, SEM, and EDX, revealed that Bg were successfully incorporated on Cmp matrix and the desired structural characteristics were present. The scaffold showed notable porosity, water retention profiles. Also, antimicrobial activity against various strains of microbes, assuring the efficacy of infection prevention. The cell-biocompatibility assay used to evaluate the scaffold's efficiency in preserving cell viability, more than 100% and osteogenic potential on Swiss 3T6 fibroblast cells. Additionally, in vitro bioactivity study ensured a direct chemical connection with the living host bone through extracellular matrix mineralization. This finding suggested that the developed composite scaffold offers a practical approach for potential bone regeneration and repair treatment.

1. Introduction

Bone possesses a remarkable capacity for self-healing, certain complex defects necessitate the use of grafts to facilitate proper recovery. However, conventional grafting methods often face significant hurdles, including chronic pain, risk of infection, host rejection, and poor integration with surrounding tissues [1]. These limitations have driven the medical community toward the development of synthetic scaffolds as a more effective alternative for bone tissue engineering. By acting as a supportive substrate, these specialized scaffolds promote cell adhesion and proliferation, which are critical steps for successful bone healing and tissue integration [2]. As a result, bone tissue engineering with biomaterials has become a viable strategy for bone defect regeneration and repair. Biocompatible polymers have a number of benefits, including adjustable mechanical characteristics, biocompatibility, and the capacity to be processed into scaffolds, films, and hydrogels, among other forms. While bone possesses a remarkable capacity for self-healing, certain complex defects necessitate the use of grafts to facilitate proper recovery.

Pullulan (PL) has emerged as a standout natural polymer in tissue engineering application. On the other hand, PL, a non-ionic polysaccharide produced by various strains of *Aureobasidium pullulans*, has also been considered as a potential BTE material because of its non-toxicity, biodegradability, high water-absorbing, and non-carcinogenic properties [3]. Scaffolds made of PL serve as a makeshift dwelling. The PL gradually breaks down as the cells multiply and the bone starts to calcify, leaving behind just natural, healthy bone. By doing this, a second surgery to remove a permanent implant is prevented. Due to the availability and non-ionic nature, it can functionalized to different forms, especially, Carboxymethylation, which will be led to the increased solubility of PL.

In recent years, the integration of bioactive nanofillers into scaffolds has significantly advanced in cell attachment, growth, and specialization, ultimately accelerating the restorative process of bone [4]. Bg stands out among these fillers for its unique capacity to interface with biological tissues and catalyze the formation of a surface hydroxyapatite (HAp) layer upon exposure to physiological fluids. When incorporated, Bg not only facilitates more rapid and robust bone repair but also reinforces the scaffold's structural integrity, rendering it far more effective for use in load-bearing skeletal regions. In this study, PL and Bg were combined to formulate optimal, porous composite scaffolds using the freeze-drying process. To ascertain these scaffolds' clinical potential in bone tissue engineering, assessments of their

biocompatibility, degradation rate, antibacterial qualities, and calcium mineralization were conducted in addition to assessments of their structural and chemical, physical, and mechanical properties. However, the addition of Bg nanofiller to Cmp has a synergistic effect that may greatly enhance the biological and physicochemical characteristics. In this work, novel porous Cmp-Bg scaffold was synthesized and characterized by XRD, FTIR, SEM and EDX techniques. Moreover, the scaffold's mechanical strength, porosity, swelling, biodegradability, cytotoxicity, antibacterial activity, and hydroxyapatite deposition were all analyzed to determine whether it is suitable for BTE application.

2. Experimental

2.1 Materials and methods

The pure form of Pullulan (PL) was purchased from Sigma Aldrich Co. Ltd. Ethanol, iso propyl alcohol, sodium hydroxide pellets, mono-chloro acetic acid, tetraethyl orthosilicate (TEOS), calcium nitrate tetrahydrate, triethyl phosphate (TEP), and sodium nitrate were purchased from Merck. Swiss albino mouse embryo tissue cells obtained from NCCS, Pune, India. The ATCC microbial strains were collected from HiMedia Laboratories, Mumbai, India. All other chemicals used were of analytical quality.

PL undergo carboxymethylation to form Cmp. For that PL, NaOH and mono- chloro acetic acid ($ClCH_2COOH$) were utilized in a 1:5:5 ratio. The procedure including, PL powder dispersed in isopropyl alcohol, then NaOH solution and an aqueous solution of mono- chloro acetic acid solution were added slowly to the reaction mixture at 70^0C. Then the carboxymethylated derivative underwent dialysis for 3 days. The produced yield was filtered and washed with deionized water and ethanol and dried at 45^0C.

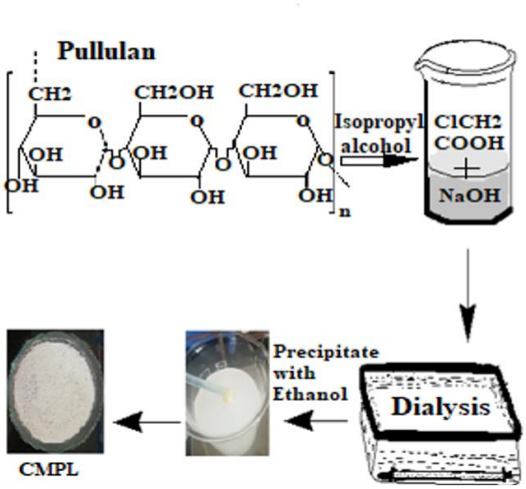

Figure 1: Schematic representation of synthesis of Cmp.

The 45S5 Bg was prepared by sol–gel synthesis using the protocol adapted from the article of Faure *et al.*, 2015 [5]. For that, The molar ratio of TEOS, TEP, calcium nitrate tetrahydrate and sodium nitrate precursors was calculated as per the molar ratio of SiO_2, CaO Na_2O, and P_2O_5 in 45S5 Bg. Initially, 2M of HNO_3 solution was taken in the 100-mL beaker. Then, TEOS and TEP were added dropwise manner. Then, $NaNO_3$ powder and $Ca(NO_3)_2.4H_2O$ powder were introduced slowly to the solution until the complete dissolution attained. After that, the mixture was ultra-sonicated to form a glassy-transparent gel. The formed gel was then transferred into crucible and dried. Finally, the dried gel was sintered at 700°C in a muffle furnace.

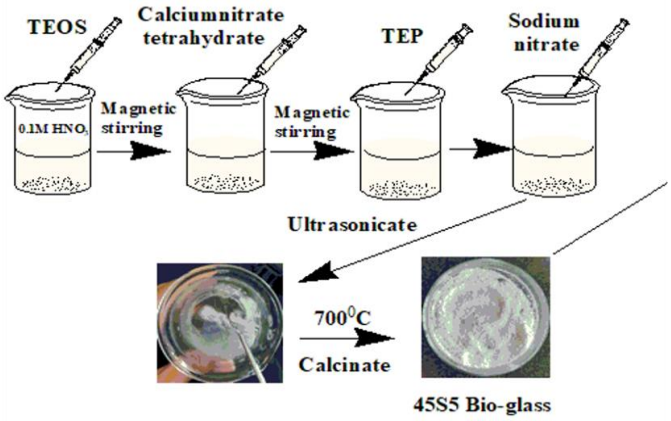

Figure 2: Schematic representation of preparation of Bg NPs.

The porous scaffolds of Cmp (control) and Cmp-Bg were fabricated by the freeze- drying process. The 2 wt.% Bg NPs with respect to Cmp concentration (0.06g) was added to the Cmp suspension Then, the mixture was ultrasonicated at room temperature until uniform dispersion of Bg NPs over a Cmp network was obtained. After that, the resulting mixtures were transferred to 24 well plates and kept for deep freezing. The frozen samples were freeze-dried at −50 °C to produce Cmp-Bg scaffold.

2.2 Characterization

The developed scaffolds (Cmp and Cmp-Bg) and, Bg NPs were confirmed by XRD (Bruker AXS-D8 advance X-ray diffractometer) and FTIR (Bruker TENSOR27 spectrometer). The topography and elemental composition of the Bg NPs were analysed by SEM- EDX (TESCAN VEGA3). A universal testing machine (FSA, M-100) with a crosshead speed of 3 mm/min and a load cell of 100 kN was used to estimate the compression strength of films in accordance with ASTM standard D695–96. The PBS (Phosphate-buffered saline) comprising 5mg of lysozyme at 37^0 C was used for analysing swelling and biodegradation kinetics of the scaffolds for the duration of 1-day and 28- days, respectively. The liquid displacement method was used to assess the porosity of the scaffolds. The antimicrobial activity of the scaffolds was estimated against *E. Coli*, and *C. Albicans*. The cytocompatibility of the scaffolds were evaluated using the Swiss 3T6 fibroblast cells. Biomineralization studies was conducted in SBF (stimulated body fluid) at a fixed interval of time.

3. Result and Discussion

3.1 Characterization of Cmp-Bg scaffold

The formation of Bg NPs was confirmed by FTIR. The wide distinctive band at 3215 cm^{-1}, which indicates that the 45S5 Bg contains various kinds of hydroxyl groups. The band around 970 cm^{-1} belongs to the stretching vibration the Si-O bond (non-bridging). The siloxane bond (Si-O-Si) of silicate network structure was confirmed by the band at band 833 cm^{-1} (Symmetric stretching vibration of Si-O-Si bond). The peaks at

671 cm^{-1} and 577 cm^{-1} due to the P-O bending vibration in $(PO_4)^{3-}$ tetrahedral units [6], respectively, these peaks indicate the successful synthesis of Bg NPs. The prepared carboxymethyl pullulan verified by the broad characteristic band around 3390 cm^{-1} is due to the hydroxyl group (O-H) stretching vibration. The characteristic band at 1631 cm^{-1} (Asymmetric stretching vibration of COO^- group), indicating the successful substitution of carboxymethyl group on the pullulan structure. The band at 1176 cm^{-1} was associated with C–O–H and C–O–C stretching of the ether bond and glycosidic linkages, respectively [7].

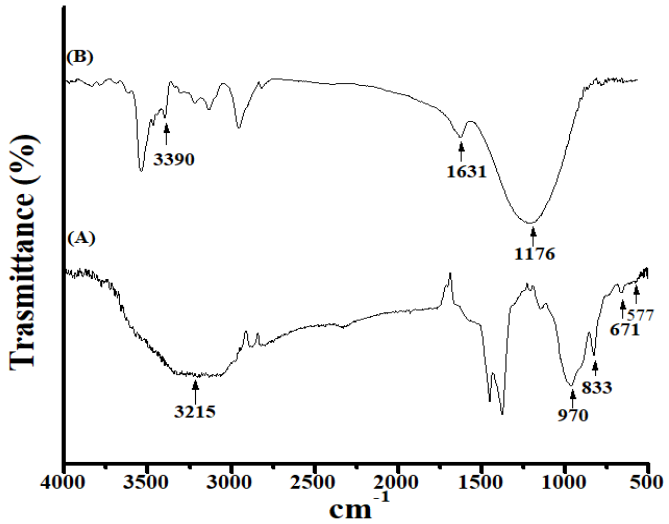

Figure 3: FTIR spectrum of [A]. Bg and [B]. Cmp.

The diffractogram of Bg NPs was displayed in the Fig. 4A. Sintering was ineffective below 700 °C, and it also reduced the particle's crystallinity [8]. The crystalline phases of maximum diffractions were observed by the peaks at 2θ angle- 21.6^0, 24.7^0, $29.523.3^0$, 33.2^0, 34.4^0, 39^0, 44.8^0, 48.7^0 and 49.7^0 consequents to the hexagonal structure of $Na_2CaSi_2O_6$ (combeite) phase (JCPDS-ICDD 01-077– 2189) [5]. The diffractive peaks of $Na_2Ca_4(PO_4)_2SiO_4$ (silicorhenate) phase was coexisted at 22.1^0, 23.3^0, 32.1^0, and 44.8^0 angle (JCPDS-ICDD 29–1193) [9]. The CMP diffractogram was shown in the Fig.4B. The amorphous nature of CMP is responsible for a broad, abrupt peak at the 2° angle in the 23.1^0 region. These findings align with those of earlier research on calcinated 45S5 Bg [8]. The diffractogram of Cmp-Bg Scaffold shows (Fig. 4C), the control peak was gradually diminished, and the BG crystalline peaks steadily emerged. According to this results, Bg NPs were successfully incorporated onto the Cmp matrix's surface.

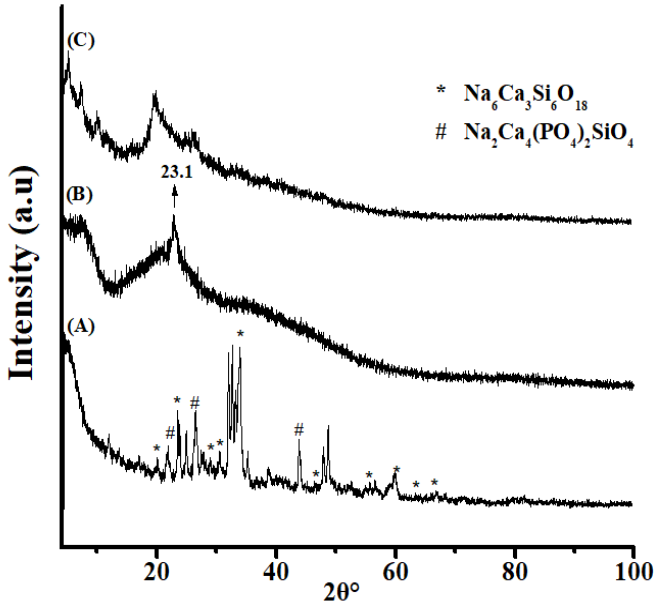

Figure 4: X-ray diffractogram of [A]. Bg, [B]. Cmp,, [C]. Cmp-Bg.

EDAX Spectra was identified the percentage of constituents such as, Si, Na, Ca, and O present in the 45S5 silica network shown in the Fig. 5A. The scaffold's surface topography is crucial because it acts as a template for cell adhesion and nutrients delivery [10]. The structural morphology of 45S5 Bg reveals particles with an average size of around 160 nm, that are spherical and irregular in shape (Fig.5A). The morphology of BG showed a high degree of agglomeration, which is typical when the material sinters at a high temperature (700^0C). The SEM images of Cmp (Fig. 5B) presented interconnected pores of surface with the average pore size of 114.5± 8.9 (Table.1). The presence of Bg NPs within the Cmp matrix resulted a rough surface with interconnecting pores (Fig. 5C) with the average pore size of 98.9 ±5.7 nm (Table.1). The porosity (%) of developed scaffold was analysed by liquid- displacement process. Consequently, the porosity of Cmp and Cmp-Bg was around 87.4 ± 3.86% and 68.8 ± 42, respectively (Table.1), which indicates the porosity decreased with the incorporation of Bg NPs. When Bg NPs are added to the Cpm matrix, it becomes more viscous when wet, which lessens the creation of pores during the freeze-drying process.

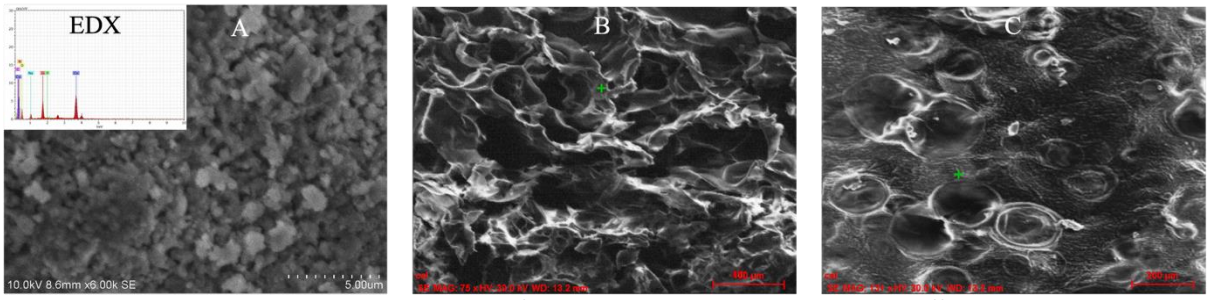

Figure 5: SEM- morphology of [A]. Bg, [B]. Cmp, and [C]. Cmp-Bg Scaffolds.

3.2 Mechanical properties

The BTE materials should possess a sufficient degree of mechanical strength in order to withstand structural integrity and bear the external pressure, it must be resilient to the affected area throughout the healing time. The compressive strength of Cmp and Cmp-Bg accordingly, 0.841±.0.02 MPa and 3.73±0.04 Mpa, respectively (Table.1). The compressive

strength of scaffolds was increased with the addition of Bg Nps, thereby it increases the overall durability.

Table 1: Types and composition of Cmp-Bg scaffolds.

Types of Scaffolds	Porosity (%)	Average Pore Size (μm)	Compressive Strength (MPa)
Cmp	87.4 ± 3.86	114.5± 8.9	0.841±.0.02
Cmp-Bg	68.8 ± 4	98.9 ±5.7	3.73±0.04

3.3 Swelling and biodegradation profile

The primary role of scaffold with adequate swelling degree is to facilitate the diffusion of life-sustaining molecules. Swelling makes it possible for growth hormones and signalling proteins to pass through the matrix, which is crucial for the recruitment of osteoblasts. Figure. 6, presented the swelling analysis of Cmp and Cmp-Bg was around 90% and 60%, respectively. The enhanced swelling behaviour was observed in PBS and attained the equilibrium after 12 hours of incubation. The higher porosity and pore size in the control scaffold might be reason for its increased swelling degree of control sample. This is explained by the inter-polymer mobility that results from immersion in aqueous fluids [11].

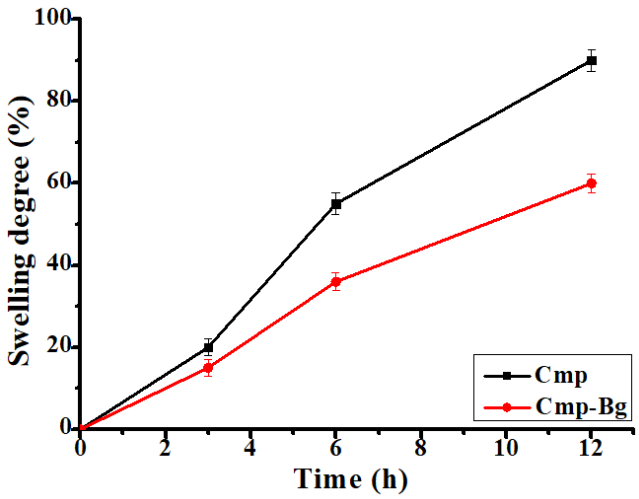

Figure 6: Swelling analysis of [A]. Cmp, and [B]. Cmp-Bg Scaffolds.

The scaffold's ultimate purpose in BTE is to act as a temporary template rather than to last forever. If the scaffold degrade too quickly, the new bone won't be able to sustain the load before it collapses. Weight loss of Cmp and Cmp-Bg scaffolds demonstrated 90% and 58% after 28 day of incubation in PBS- Lysosome system [12] (Fig. 7). The interaction of Bg NPs with the Cmp polymer matrix may limit the degradation of the Cmp-Bg scaffold in the PBS medium, leading to controlled degradation in comparison with to the Cmp. The ionized COOH group in the Cmp shows complete dissolution in PBS solution. It could result from both the hydrophilicity and an increase in the pores of Cmp scaffold.

3.4 Antimicrobial activity

Implanted associated infections are most common reason for BTE failure. To create improved antimicrobial surfaces, it is essential to comprehend this failure mechanism. In this study, the microbicidal activity of the Cmp and Cmp-Bg was evaluated against *E. Coli* (Gram -ve bacteria), *S.* and *C. Albicans*. As shown in Fig.8, Cmp-Bg presented the higher inhibition zone 21mm and 20.5 mm, respectively, compared to the Cmp Scaffold. This is due to the presence of Bg NPs. The Bg in the scaffold experiences a quick ion exchange when immersed in bodily fluids. The H^+ and H_3O^+ ions from the surrounding fluid take the place of Na^+ and Ca^{2+} ions from the glass. The pH rises locally due to this ion exchange, making the surroundings more alkaline. In high pH, the majority of harmful microbes cannot survive or proliferate [13].

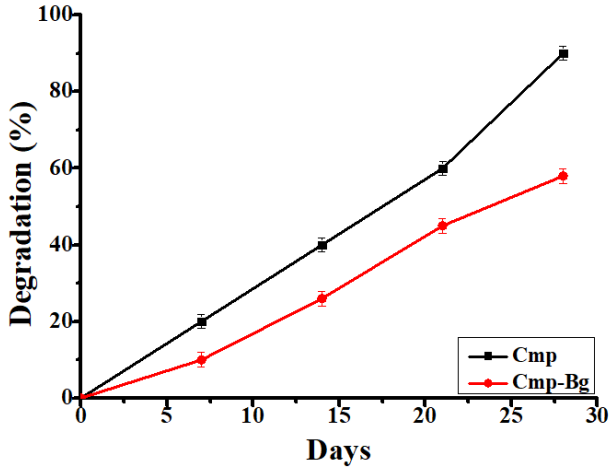

Figure 7: Bio-degradation of analysis of [A]. Cmp, and [C]. Cmp-Bg Scaffolds.

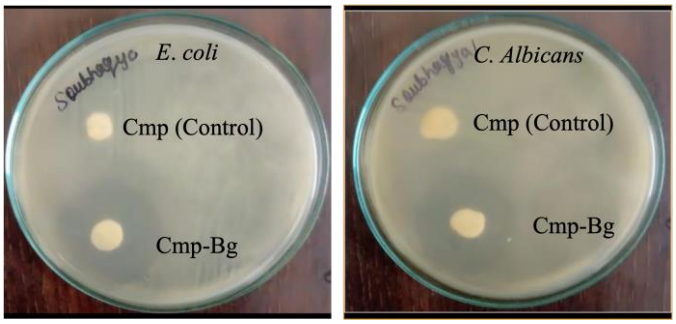

Figure 8: Antimicrobial activity of control Cmp and Cmp-Bg scaffolds against (A) *E. Coli*, (B). *C. Albicans*.

3.5 Cytocompatibility analysis

The cytotoxicity of Cmp-Bg scaffold was evaluate by the MTT assay using Swiss 3T6 fibroblast cells (Fig.9). In this analysis, after 48 hours of incubation, the Cmg-Bg scaffold demonstrated an enhanced cell viability compared to the cmp and +ve control. The cell viability of Cmp and Cmg-Bg was found to be 100% and 109%, respectively. The -ve control (Triton X-100) demonstrated the reduced cell viability as expected. These findings indicated that Cmg-Bg could be suitable for cell proliferation.

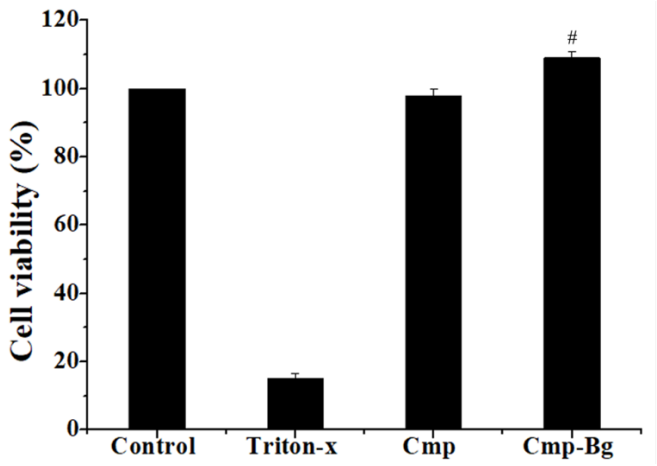

Figure 9: Biocompatibility of Cmp and Cmp-Bg Scaffolds against Swiss 3T6 fibroblast cells [# describes a substantial difference compared to the negative control ($p < 0.05$)].

The aim of bio-mineralization study is the formation of Hap (hydroxyapatite) layer, which shares structural and chemical similarities with the mineral phase of natural bone. The Bg from Cmp-Bg scaffold binds to living bone tissue when it comes into contact with body fluids, therefore, BG is referred to be "bioactive". The bio- activity of the Cmp-Bg scaffold with physiological fluid (SBF solution) was evaluated for 21 days. Following immersion in the SBF, the sample's morphology shows clearly noticeable changes in the SEM micrograph shown in the Fig.10. After soaking the scaffold in SBF for distinctive time intervals (1-21 days), it was observed that, the pH range has instantly increased about (pH -8) due to the release of Na^+ and Ca^{2+} ions exchanged with ions in the SBF (H^+/H_3O^+) [14]. After 14 days of immersion, the pH was found to have reached around 7.4 and persistent for 21 days. It appears that the sample's weight increased to 170 mg; this could be due to the formation of hydroxyapatite layer on the scaffold surface.

3.6 Biomineralization analysis

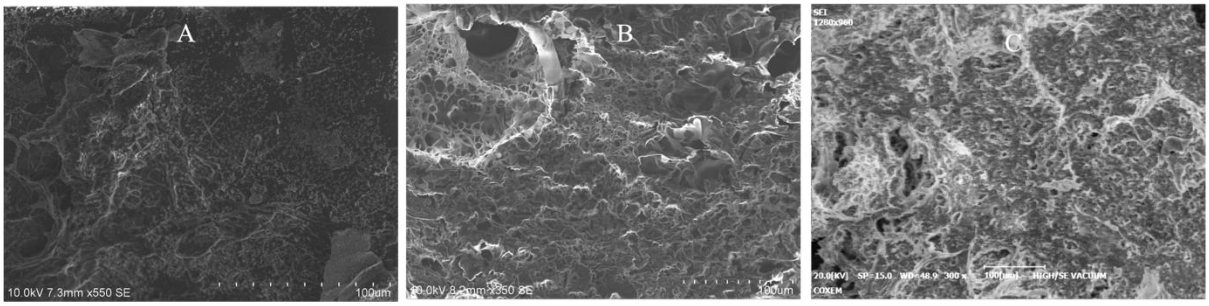

Figure 10: Morphology of Cmp-Bg Scaffold after being treated with SBF for (A) 0, (B) 7, (C) 14 and (D) 21 days.

4. Conclusions

A nominal composition of 45S5 bioactive glass incorporated with carboxymethyl pullulan (Cmp) 3D- porous scaffold was formulated by freeze-drying for the application of bone tissue Engineering. The FTIR, XRD, SEM, and EDX techniques confirmed successful integration of Bg into the Cmp matrix, showing desired chemical, structural features. SEM images revealed a rough surface with interconnected pores; porosity decreased from about 87% in Cmp to 69% in Cmp-Bg due to Bg addition affecting pore formation during freeze-drying. Incorporation of Bg nanoparticles significantly increased compressive strength from 0.841 MPa in Cmp to 3.73 MPa in Cmp-Bg, enhancing scaffold durability for load-bearing applications. The Cmp scaffold showed higher swelling (~90%) compared to Cmp-Bg (~60%), while biodegradation after 28 days was 90% for Cmp and 58% for Cmp-Bg, indicating controlled swelling and degradation rate with Bg presence. The Cmp-Bg scaffold exhibited greater inhibition against *E. coli* and *C. Albicans*, presenting their suitability for anti-microbial activity. MTT assay against Swiss 3T6 fibroblast cells showed enhanced cell viability (109%), indicating appropriateness for supporting cell proliferation. Immersion in SBF demonstrated hydroxyapatite deposition on the Cmp-Bg scaffold surface over 21 days, with pH changes consistent with bioactive glass ion release and bone-like mineral formation. These results confirmed that Cmp-Bg scaffold could be used as a potential Osteoconductive framework for BTE application.

Authors' contributions

All authors contributed equally to the conception, design, experimental work, data analysis, interpretation of results, and preparation of the manuscript. All authors reviewed and approved the final version of the manuscript for publication.

Conflicts of interest

The author declares no conflict of interest.

Funding

This research received no external funding.

Data availability

No new data were created.

References

[1] P.J. Kondiah, Y.E. Choonara, P.P. Kondiah, et al., A review of injectable polymeric hydrogel systems for application in bone tissue engineering, *Molecules* **21** (2016) 1580.
[2] K.K. Mallick, S.C. Cox, Biomaterial scaffolds for tissue engineering, *Front. Biosci*. (Elite Ed.) **5** (2013) 341–360.
[3] M. Manivannan, S. Sathiya Nathan, P. Sasikumar, L. Ramkumar, D. Navaneethan, P. Prabu, F.M. Anjalin, N. Dharamraj, M.S. Alqahtani, M. Abbas, Review on applications of pullulan in bone tissue engineering: Blends and composites with natural and synthetic polymers, *Polym. Polym. Compos*. **31** (2023) 1–13.
[4] L. de Siqueira, R.F. Gouveia, L. Grenho, et al., Bioactive and biomimetic behavior of polymeric composites for tissue engineering applications, *J. Mater. Sci*. **53** (2018) 10718–

10732.
[5] J. Faure, R. Drevet, A. Lemelle, N. Ben Jaber, A. Tara, H. El Btaouri, H. Benhayoune, A new sol–gel synthesis of 45S5 bioactive glass using an organic acid as catalyst, *Mater. Sci. Eng. C* **47** (2015) 407–412.
[6] H. Pirayesh, J.A. Nychka, Sol–gel synthesis and characterization of bioactive glass materials, *J. Am. Ceram. Soc*. **96** (2013) 1643–1650.
[7] G. Mocanu, D. Mihai, D. LeCerf, L. Picton, G. Muller, Synthesis of new associative gel microspheres from carboxymethyl pullulan and their interactions with lysozyme, *Eur. Polym. J*. **40** (2004) 283–289.
[8] L. Lefebvre, J. Chevalier, L. Gremillard, R. Zenati, G. Thollet, D. Bernache-Assolant, A. Govin, Structural transformations of bioactive glass 45S5 with thermal treatments, *Acta Mater*. **55** (2007) 3305–3313.
[9] J.R.J. Delben, K. Pereira, S.L. Oliveira, L.D.S. Alencar, A.C. Hernandes, A.A.S.T. Delben, Bioactive glass prepared by sol–gel emulsion, *J. Non-Cryst. Solids* **361** (2013) 119–123.
[10] D.M. Escobar-Sierra, J.S. Posada-Carvajal, D.L. Atehortúa-Soto, Fabrication of chitosan/bioactive glass composite scaffolds for medical applications, *Rev. Fac. Ing. Univ. Antioquia* **80** (2016) 38–47.
[11] A.S. Soubhagya, A. Moorthi, M. Prabaharan, Bioactive polymeric scaffolds for bone tissue engineering applications, *Int. J. Biol. Macromol*. **157** (2020) 135–145.
[12] P. Kumar, B.S. Dehiya, A. Sindhu, Comparative study of chitosan and chitosan–gelatin scaffold for tissue engineering, *Int. Nano Lett*. **7** (2017) 285–290.
[13] A. Trishala, C. Jacob, The anti-bacterial activity of bioactive glass, *Int. J. Adv. Res*. **4** (2016) 1070–1077.
[14] T. Kokubo, Design of bioactive bone substitutes based on biomineralization process, *Mater. Sci. Eng. C* **25** (2005) 97–104.